PERGAMON

International Journal of Heat and Mass Transfer 45 (2002) 237–253

International Journal of HEAT and MASS TRANSFER

www.elsevier.com/locate/ijhmt

Spatio-temporal analysis of nucleate pool boiling: identification of nucleation sites using non-orthogonal empirical functions

Patrick E. McSharry [a,b], Jerome H. Ellepola [b], Jost von Hardenberg [a,b], Leonard A. Smith [a], David B.R. Kenning [b,*], Kevin Judd [c]

[a] *Mathematical Institute, University of Oxford, Oxford OX1 3LB, UK*
[b] *Department of Engineering Science, University of Oxford, Parks Road, Oxford OX1 3PJ, UK*
[c] *Department of Mathematics and Statistics, University of Western Australia, Nedlands, WA 6907, Australia*

Received 18 December 2000; received in revised form 30 April 2001

Abstract

The analysis of spatio-temporal data and the physical understanding of the systems generating them are often limited by the available techniques. These limitations are especially evident in nucleate boiling. This paper investigates the analysis of a sequence of temperature fields obtained from a pool nucleate boiling experiment. Spatio-temporal data for the wall temperature in pool nucleate boiling of water on a thin, horizontal, stainless steel plate were obtained by liquid crystal thermography and high speed video recording. A previous analysis provided examples of the thermal conditions for activation of individual nucleation sites, for the heat transfer mechanisms during bubble growth and for the consequent interactions between adjacent sites. Principal component analysis (PCA) is shown to provide a reconstruction of the temperature fields that is accurate in the root mean square sense but which obscures information about the underlying physics, such as positions of the nucleation sites. In contrast, a new approach using non-orthogonal empirical functions (NEFs) encodes the relevant physical constraints (e.g., each NEF has a radially symmetrical form as suggested by the pattern of cooling during bubble growth). NEFs provide an efficient identification of the positions of active sites in successive frames; they are better suited to the analysis of non-stationary dynamics than PCA and allow for information compression.

1. Introduction

The need for the analysis of spatio-temporal complex datasets emerges in a wide range of fields in the natural sciences and engineering. Typically the processes generating the data are inherently non-linear, limiting the applicability of classical linear analysis techniques for isolating the basic processes at work and for modelling the data. The principle of linear superposition is at the heart of many traditional techniques: the sum of two solutions is also a solution. This need not be the case if the dynamics are non-linear and the variance "captured" need not reflect information.

Nucleate boiling represents an example in which the underlying processes are strongly non-linear and not completely understood. Better understanding of the information available from spatio-temporal experiments is required to advance our current understanding of the physics of nucleate boiling, thereby allowing improved industrial applications. Better representations of the data are a necessary first step, where "better" means techniques which improve visualization of the key processes, the identification of physical processes, and the modelling of their dynamics. This paper contrasts two methods for representing spatio-temporal data, traditional empirical orthogonal functions (EOFs) and newly

* Corresponding author. Tel.: +44-1865-273-000; fax: +44-1865-273-010.
E-mail address: david.kenning@eng.ox.ac.uk (D.B.R. Kenning).

0017-9310/02/$ - see front matter
PII: S0017-9310(01)00152-1

Nomenclature

a_k	coefficient of the kth basis function in the NEF reconstruction (9)
$C_{\mathrm{LS}}(t)$	least-squares distance between the model and the reconstruction at time t; defined in (10)
$C(K)$	cost function for the NEF algorithm, when K basis functions are used; defined in (11)
$\mathbf{E}^{(K)}(t)$	model reconstruction error at time t, when K basis functions are used (a vector of length N)
$\mathbf{G}(t)$	observed data at time t (a vector of length N)
$\hat{\mathbf{G}}^{(K)}(t)$	reconstruction of data at time t, using K basis functions (a vector of length N)
K	number of basis functions used for the reconstruction
L	number of possible basis functions (NEFs) in $\mathscr{V}$
M	number of pixels per frame
N	number of data frames
R	radius of a NEF basis function
t	time
x	horizontal coordinate
y	vertical coordinate
$\mathscr{V}$	pool of basis functions which can be selected by the NEF algorithm; defined in Appendix A

Greek symbols

α	penalty coefficient for $C(K)$, as used in (11)
$\boldsymbol{\mu}$	projection of the error field onto the pool of basis functions $\mathscr{V}$
Φ	NEF basis function (a vector of length N)

Superscript

T	transpose of a vector or matrix

devised non-orthogonal empirical functions (NEFs). It is shown how both are useful and that for nucleate boiling NEFs are more so for the aims noted above.

After an introduction to the classical method of principal component analysis (PCA), this paper demonstrates the new NEF method for analysing time-varying spatial fields, which is applied to experimental data obtained by liquid crystal thermography during pool nucleate boiling on a thin horizontal plate [1].

The layout of this paper is as follows: Section 2 discusses the need for spatio-temporal descriptions of nucleate boiling, both in experiments and in numerical models, and reviews the small amount of work so far done in this respect. Section 3 describes the experimental setup and the data used in this paper. Section 4 provides a brief introduction to PCA. Section 5 introduces the novel idea of NEF analysis and its application to nucleate boiling. An analysis of the experimental data with this new technique is presented in Section 6. Finally Section 7 discusses the main differences between PCA and NEF analysis and possible future developments.

2. Spatio-temporal description of nucleate boiling

Nucleate boiling, usually combined with convection, is employed industrially when high heat fluxes have to be transferred from a solid wall to a liquid at low temperature differences. Applications range from evaporators in power stations and refrigeration plant to the cooling of micro-electronic devices. They cover an extremely wide range of fluids, geometries and flow conditions. Currently, designers have to use rather inaccurate empirical correlations that relate heat flux and wall superheat as spatio-temporally averaged quantities for steady-state conditions. These correlations may be restricted to particular regimes and separate criteria are required for transitions between regimes. Furthermore, non-dimensional analysis cannot be applied rigorously, because of the large number of potentially significant variables. A way out of this difficulty has been to exploit the scaling of fluid properties with reduced pressure, by scaling the heat transfer coefficient to standard conditions at a reference reduced pressure [2]. It remains difficult to incorporate the sensitivity of nucleate boiling to the surface condition, bulk properties and thickness of the heated wall. The average surface roughness, R_{a}, provides only a weak guide to bubble nucleating characteristics [3] and may be expected to interact with the wall bulk properties, leading to increasingly complicated empirical correlations. New methods of measuring and processing two-dimensional surface roughness may lead to the specification of more relevant parameters [4] and eventually, along with other methods such as gas bubble nucleation [5], to the identification of potential nucleation sites. With this information available, it may be advantageous to supplement correlations by numerical models that are the best available representations of the very complicated physical processes in nucleate boiling. Because of the imperfect understanding of these processes, it may be some time before models replace empirical correlations, but models can be used to examine conditions that correlations cannot, such as (i) the hysteresis and "patchy" development associated with boiling inception, (ii) transitions between regimes following gradual changes in

heat flux and (iii) local fluctuations in wall temperature during steady-state boiling. These conditions may affect the cooling of electronic components, the heating of sensitive fluids and the development of thermal stresses.

Older models for nucleate boiling, e.g., [6], assumed a uniform and constant wall superheat, thus excluding any influence of wall bulk properties and thickness, despite the inherently non-uniform and unsteady nature of the heat transfer processes. More recent models, for an axi-symmetrical cell round a single bubble site, calculate the cyclical variations in wall temperature during bubble waiting time, growth and departure [7–9]. Such models presuppose regular, periodic production of bubbles at an "average" nucleation site. Real boiling is known to be more complicated. Bubbles from a given nucleation site may have a distribution of sizes and waiting times; sites differ in activity and their spatial distribution is not uniform; bubbles may coalesce, even at low heat fluxes.

The spatio-temporal variations in wall temperature have been demonstrated in experimental studies of nucleate boiling by liquid crystal thermography. Watwe and Hollingsworth [10] followed the irregular development of nucleate boiling on a horizontal plate and its interaction with circulation in the surrounding liquid pool. High speed video recording of the liquid crystal colourplay with simultaneous recording of the bubble motion makes it possible to measure the local variations in wall temperature associated with individual bubbles. The cyclic variations in wall superheat at individual sites have been measured during the boiling of water on horizontal [1] and vertical [11,12] plates. Individual sites nucleate at different superheats: bubble growth causes local cooling and the next bubble nucleates when the superheat is recovered. There are small variations in the nucleation superheats for different bubbles at the same site, the reason for which is not yet known: they do not appear to be caused by the local temperature gradient in the liquid phase, so either the residual vapour may settle at different metastable positions in a cavity or there may be several closely spaced cavities that appear as a single site. The cooling associated with bubble growth and departure is confined to the contact area between the bubble and the wall: there is no direct cooling over a larger area of influence [1,12]. The collective motion of bubbles after departure causes an increase in convective cooling. When bubbles move tangentially on a vertical plate [11,12] or under a sloping plate [13], their wakes initiate additional convective cooling in particular regions. The cooling caused by bubbles from one site influences the thermal conditions at other sites, causing intermittent bubble production or suppression [1,11,12]. Sites may also interact by (i) bubble coalescence [14], (ii) seeding or displacement of vapour from unstable sites [15] and (iii) other fluid dynamical interactions that are less readily detectable from the variations in wall temperature and observations of the bubbles.

If the interactions between sites occur frequently, it may be necessary to use multi-site, rather than single-site, models. The detailed analysis of examples of interactions is extremely time consuming as the assessment of their significance requires the identification of many examples over long periods of observation. At low heat fluxes, the positions of the nucleation sites can be confirmed by observations of the bubbles and the analysis can be confined to the temperature–time measurements at the sites. The interactions between a small group of sites on a horizontal plate over a short period were laboriously identified in [1]. In [16], by assuming that a sudden decrease in temperature exceeding a specified threshold signalled either local nucleation or cooling by a bubble from an adjacent site, probable interactions were identified from near-simultaneous decreases at pairs of sites in the same group. It was shown that over a longer period the frequency of coincidences was much greater than would be expected for random events. At higher heat fluxes, the view of the bubbles is obscured and the positions of active sites and their interactions can only be deduced from observations of the liquid crystal over a long period. This is one motive for developing economical methods of analysing long sequences of two-dimensional temperature fields deduced from high speed video recordings.

Time-resolved liquid crystal measurements are confined to the special conditions of boiling on a very thin, electrically heated wall. These conditions reduce bubble frequencies and modify features that influence the local variations in wall temperature, e.g., the thermal capacity of the wall and lateral conduction. Limited spatial resolution and frequency response [1,14] prevent an application to boiling conditions that involve very small bubbles and/or high bubble frequencies. Liquid crystal measurements also have poor signal-to-noise ratios. So far, detailed measurements have been made only for water boiling at near-atmospheric pressure. Consequently great care is necessary in extrapolating the mechanisms observed under these conditions to other conditions. Even with this reservation, the experiments provide data for the validation of numerical models over a range of conditions, which would increase confidence in the use of the models to explore conditions inaccessible to liquid crystal experiments. The experiments may not identify all the important mechanisms at the extrapolated conditions, but the onus is on a modeller who chooses to exclude a mechanism to show that its exclusion is justified.

Multi-site numerical simulations can consider temperature fields in the wall around tens or hundreds of nucleation sites of different sizes placed at irregular spacing at low heat fluxes. In this case sites produce discrete bubbles [17–19], while at high heat fluxes sites

produce vapour stems discharging into a large hovering bubble [20,21]. Such models are hybrids of calculations from first principals and empirical correlations. Conductive heat transfer within the wall is calculated numerically, using a fine grid where required. Heat transfer from the wall to bubbles or stems is described by boundary conditions that approximate micro-layer or triple-interface evaporation in circular regions around each nucleation site. Lateral motion of bubbles with wake cooling at low heat fluxes has not been considered, although some single-site models include a contribution to the heat flux from sliding bubbles [22,23]. Convection and bubble motion in the liquid–vapour region is less well understood and the modelling here is heavily dependent on empirical correlations. Attempts at simulation entirely from first principals of a wall region with many nucleation sites, fully coupled to the liquid–vapour region, are still at a pioneering stage (see, for example, the two-dimensional model of Tajima and Shoji [24] which expands on earlier work by Yanagita [25]). Multi-site models require specification of site positions and their characteristics, e.g., as effective radii, or superheats for activation and cessation. At present, these models have only been run under a limited range of conditions; it is not known how extensive a model should be, whether it is sufficient to model the interactions between tens of nucleation sites or whether thousands must be considered. Validating comparisons between multi-site models and liquid crystal experiments have yet to be made.

Such comparisons may be complicated by chaotic behaviour in modelled and real boiling over certain ranges of conditions, characterised by sensitivity of the time development of the state of the system to initial conditions and reductions in predictability of future states by deterministic modelling. Nucleate boiling systems satisfy the necessary conditions for chaos by having many degrees of freedom and non-linear dynamics, to which the switching interactions between sites are just one contribution. Smith [26,27] has noted that predictions of the developing state of a physical system by deterministic models, e.g., in weather forecasting, are limited by three separate causes: experimental uncertainty in the specification of initial conditions, imperfections in the model and the non-linear dynamics of the system. Each of these apply in nucleate boiling: liquid crystal measurements are subject to noise and the region of observation is likely to be smaller than the full extent of the system, so that there are unknown edge effects; the physical processes cannot be modelled accurately and the system is non-linear. The evidence of chaotic behaviour is reviewed briefly below. Thus it is unlikely that the measured and predicted states of a boiling system will coincide over long periods. In nucleate boiling, however, the temporal development of the state of the system is not in itself of particular interest, except in transitions between regimes. It is more important to know whether the system has an equilibrium state represented by a limit cycle, the corresponding relationship between the spatio-temporal average wall temperature and heat flux and the amplitude, spatial and time scales of the fluctuations in these quantities. Methods must be devised to measure the performance of a model in these respects and this is the second motive for developing methods to analyse the spatio-temporal data from either liquid crystal experiments or numerical simulations.

Modelling and experimental studies of chaos in boiling have been reviewed by Nelson et al. [28] and Shoji [29]. Sadasivan et al. [20] examined the single variable-time series for the fluctuations in the spatially averaged wall temperature calculated by their multi-site model, thereby using only a small part of the information generated by the calculations. They found indications of period doubling with increasing heat flux, a classical route to chaotic behaviour. Shoji et al. [29] measured the length-averaged wall temperature–time series for boiling on electrically heated platinum wires 0.8 and 2 mm long. They concluded that the series had attractors indicative of chaos, for which they calculated high fractal dimensions which were different in nucleate, transitional and film boiling. Lee [30] investigated the chaotic release of bubbles during film boiling on a wire. The study of spatio-temporal chaos requires distributed sensors that do not affect the surface conditions that control nucleate boiling. Shoji et al. [31] used five microthermocouples embedded in a thick copper wall to measure local fluctuations in near-surface wall temperature with amplitudes in nucleate boiling of order 1°C (comparable with the computations in [18] for copper). Ellepola [32] analysed simulated data and actual data from liquid crystal experiments. The time series of the temperature measurements at a single site and the series generated by a simple lumped-parameter numerical model for two interacting sites were analysed by standard means for fractal dimension and Lyapunov exponents [33] and their predictability was estimated [32,34].

3. Spatio-temporal data

The experimental data were obtained during the study of saturated pool boiling of water at atmospheric pressure on a horizontal stainless steel plate 0.125 mm thick, heated by ripple-free direct electric current to yield a heat flux of 125 kW/m^2. (For more details see [1].) At this heat flux the general production of bubbles made it difficult to view events at individual sites on the bubble side. The growth of a bubble could still be detected on the liquid crystal side by the short-lived near-circular area of cooling around its nucleation site, which caused a change in the colour of the liquid crystal. The

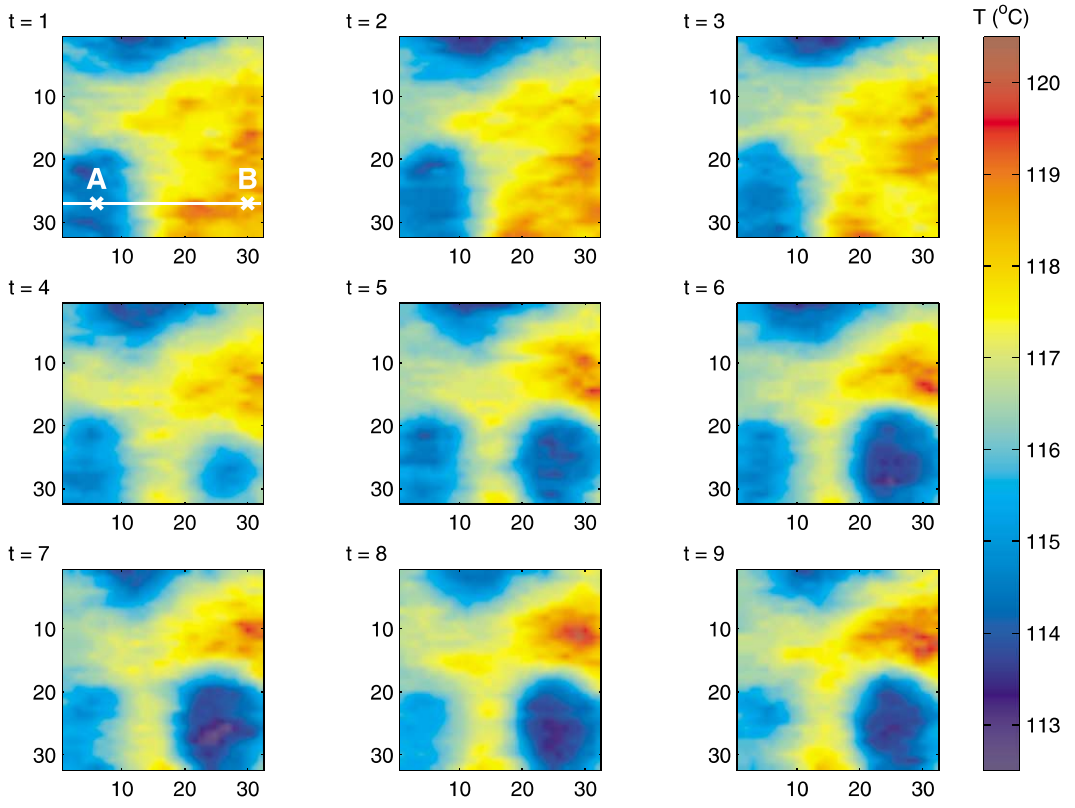

Fig. 1. The surface temperature field of the stainless steel plate for the first nine time steps. Possible nucleation sites A and B and the horizontal slice at $y = 27$ are marked in the first panel.

colourplay of the liquid crystal was recorded at 200 Hz by a colour video camera. The NTSC VHS recordings were replayed through a RGB decoder to a framegrabber with onboard 8 bit conversion to hue. A sequence of $N = 8000$ hue fields (40 s) was transferred to a PC for analysis. Each field was converted to a temperature field, using a pre-determined calibration. The analysis was confined to a small part of the experimental area, measuring 11.4 mm $\times$ 10 mm and corresponding to 64 pixels in the horizontal direction and 64 pixels in the vertical direction. In this paper, the small deviation of the aspect ratio from 1 is neglected. Alternate fields were interlaced so in any one field there were 64 pixels per row and 32 rows. For present purposes, the values at adjacent pairs of pixels in each row were averaged and the small difference in vertical positions of rows x and $x + 1$ in alternate even and odd fields was neglected, resulting in a sequence of arrays of $M = 32 \times 32$ temperatures, at time intervals of 5 ms. Nine consecutive members of the sequence are illustrated in Fig. 1.

A discrete coordinate system is defined using x and y to describe the horizontal and vertical directions, with $(x, y) = (1, 1)$ specifying the top left corner pixel. Note that nucleation sites outside the particular section shown in Fig. 1 may also give rise to changes in the temperature field outside this area. Visual inspection of the data suggests two possible nucleation sites at positions $A = (6, 27)$ and $B = (30, 27)$, marked in the first panel of Fig. 1.

Time variation in the temperature field is illustrated using a horizontal slice at $y = 27$, also marked in Fig. 1. Fig. 2 shows the temperature profile over this slice for the first 500 time steps. This slice appears to pass through the cooled areas around several nucleation sites, although not necessarily through their centres. The left-hand site appears to be much more active than the others. One of the objectives of this analysis is to determine the positions of the sites and the times at which bubbles nucleate. Variation in the frequency of bubble activity may also be seen from the temperature–time series at these two nucleation sites with approximate positions A and B shown in Fig. 3.

4. Principal component analysis

PCA [35–37] is a popular technique which aims to provide a description of spatio-temporal data in terms of

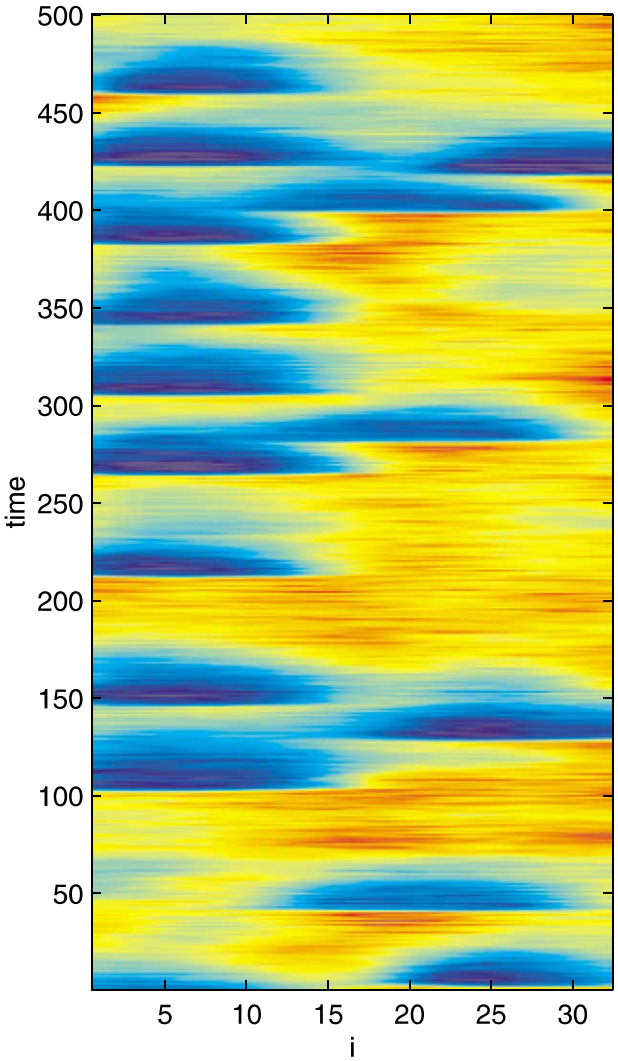

Fig. 2. The temperature field at $y = 27$ on the stainless steeel plate for the first 500 time steps. Colourmap as in Fig. 1.

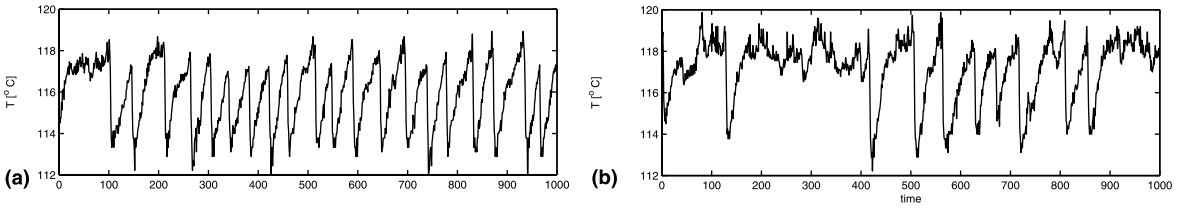

Fig. 3. The temperature on the stainless steel plate for the first 1000 time steps at sites A and B.

a relatively small number of spatial basis vectors which are constant in time. The goal is to minimise the root-mean-square reconstruction error between the reconstruction and the original field, using, say, K basis vectors.

Consider a sequence in time of spatially extended measurements $\Theta_{ij}(t)$, $(i = 1, \ldots, P,\ j = 1, \ldots, Q)$ on a spatial grid of size $P \times Q$; for example in this paper each $\Theta_{ij}(t)$ represents a temperature measurement at pixel position (i, j) on the plate and $P = Q = 32$.

For convenience each two-dimensional array of pixels, $\Theta_{ij}(t)$, can be considered a single vector $\mathbf{G}(t)$ where the kth component of $\mathbf{G}$ is $G_k(t) = \Theta_{ij}(t)$, for $k = (j-1)P + i$, $k = 1, \ldots, P \times Q$. In this paper it will sometimes be clearer to think of the measurement field as a matrix, $G_{ij}(t) = \Theta_{ij}(t)$, but there is a one-to-one correspondence between the two representations. Boldface symbols represent vectors and matrices.

PCA provides a basis for $\mathbf{G}$, representing the time dependence of $\mathbf{G}$ by a series of principal components $p_k(t)$, each of which describes the time-dependent intensity of one basis vector $\mathbf{v}_k$ constant in time. In symbols

$$\mathbf{G}(t) = \sum_{k=1}^{M} p_k(t)\mathbf{v}_k, \tag{1}$$

where the basis vectors $\mathbf{v}_k$ are called EOFs and form an orthonormal basis; the time-varying coefficients $p_k(t)$ are the principal components. M is the number of basis vectors which in general equals the number of pixels (i.e., $M = P \times Q$); as discussed below PCA is often used for "data compression" by considering the sum over the leading EOFs, i.e., to some $K < M$.

The standard procedure is as follows: first a time-averaged field is defined as

$$\bar{\mathbf{G}} = \frac{1}{N}\sum_{i=1}^{N} \mathbf{G}(t_i), \tag{2}$$

where N is the number of frames observed and t_i $(i = 1, \ldots, N)$ are the discrete times at which the data are sampled. An anomaly $\mathbf{G}'(t) = \mathbf{G}(t) - \bar{\mathbf{G}}$ is constructed by removing the time average. Next, the covariance matrix $\mathbf{S}$ is formed

$$\mathbf{S} = \frac{1}{N-1}\sum_{i=1}^{N} \mathbf{G}'(t_i)\mathbf{G}'(t_i)^{\mathrm{T}}, \tag{3}$$

where each diagonal term, S_{jj}, is the variance in the jth pixel, while off-diagonal terms, S_{jk}, are the covariances between the jth and kth pixels, thus $S_{jk} = S_{kj}$ and $\mathbf{S}$ is a symmetric matrix. An eigenvalue decomposition [36,38] yields

$$\mathbf{S} = \mathbf{V}\mathbf{\Sigma}^2\mathbf{V}^{\mathrm{T}}, \tag{4}$$

where $\mathbf{V}$ is an orthonormal matrix (i.e., $\mathbf{V}\mathbf{V}^{\mathrm{T}} = \mathbf{I}$) and $\mathbf{\Sigma}^2$ is a positive definite diagonal matrix; the positive square roots σ_k of its diagonal elements are known as the singular values of $\mathbf{S}$. The columns of $\mathbf{V}$, $\mathbf{v}_k$, are the EOFs, and the contribution which each of them gives to the total variance of the field is given by the corresponding eigenvalue σ_k^2.

Due to the orthonormality of $\mathbf{V}$, the principal components may be computed by projecting the field $\mathbf{G}(t)$ onto the EOFs,

$$p_k(t) = \mathbf{v}_k^{\mathrm{T}}\mathbf{G}(t). \tag{5}$$

By convention the diagonal elements of $\mathbf{\Sigma}$ are ordered so that $\sigma_j \geqslant \sigma_k$ for $j < k$. It follows that a hierarchy of reconstructions which capture increasing amounts of the variance may be formed by truncating the number of EOFs to $K \leqslant M$

$$\hat{\mathbf{G}}^{(K)}(t) = \sum_{k=1}^{K} p_k(t)\mathbf{v}_k. \tag{6}$$

Note that $K = M$ results in a perfect reconstruction, $\hat{\mathbf{G}}^{(M)}(t) = \mathbf{G}(t)$.

Fig. 4 shows the first eight EOFs calculated from the experimental temperature fields discussed in Section 3. Note that none of the EOFs resembles the typical field (see Fig. 1) formed by a single active nucleation site during bubble formation. The constraint of orthogonality on the EOFs need not yield a sparse representation of the data in terms of separate cooling regions, although such a separation would be appropriate for nucleate boiling temperature data. Furthermore, PCA employs a superposition of EOFs to reconstruct the original data; since local cancellation between different EOFs is used to represent a single physically meaningful pattern, more than one EOF may be necessary to reconstruct the temperature field associated with just one nucleation event.

Fig. 5(a) shows the associated singular value spectrum and the fraction of the variance which is explained by using K EOFs is shown in Fig. 5(b). When PCA is used to compress the data, these plots are used to choose the number of EOFs needed to achieve a specific level of compression, as defined by the fraction of the variance reconstructed. In the present case the first 10 EOFs capture 90% of the variance in the data and more than 60 EOFs are required to capture 98%. The decision on the appropriate level of compression in a given case is not straightforward. The EOFs with smallest singular values are commonly thought to have lower signal-to-noise ratios, hence a large part of the variance may be caused by measurement noise, rather than physical events; in this case truncation of the set of EOFs would be advantageous. The same EOFs, however, may contain information about important but relatively infrequent nucleation events. EOFs provide a powerful means of compressing data in terms of variance but may not provide direct insight into the physical processes that create the fields. The point here is that, while capturing variance is a reasonable goal in linear stochastic systems, doing so need not reflect the information content in non-linear streams of data, as discussed in the next section.

5. Non-orthogonal empirical functions

Variance compression need not be a fundamental aim when dealing with non-linear systems, and there are numerous uses for which EOFs are not ideal as basis

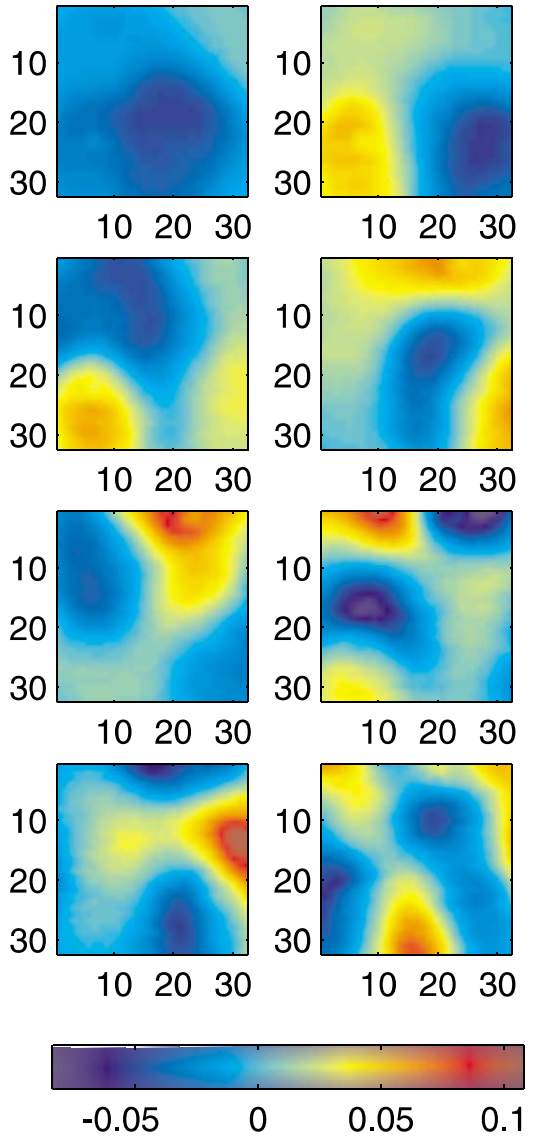

Fig. 4. The first eight EOFs of the temperature fields, in order of decreasing singular values, row by row, from top left to bottom right.

vectors. Nucleate boiling may prove to be one such system. Bubbles develop at specific nucleation sites before disengaging from the surface. By monitoring a temperature field of the surface, the bubble growth manifests as a sharp drop in temperature around the nucleation site over an approximately circular region, followed by a more gradual recovery of the temperature. The circular region may be overlapped by the effects of bubble growth at other sites. A basis which reflects the existence of the individual localised nucleation sites and uses the approximate radial symmetry of the bubbles may offer a much more efficient method of describing the dynamics. This approach also encodes some of the underlying physics in the analysis, rather than blindly applying statistical methods to the data. Basis functions which are radially symmetric around the nucleation sites, with a fixed shape, but varying radius represent a natural choice for this purpose. In general such a basis would not have the property of orthogonality of the EOF basis; it is not constructed to be efficient in capturing variance like EOFs, but it may be better at describing the physics.

As an example consider NEFs with a radially symmetric quadratic structure

$$\Phi(\mathbf{x};\mathbf{x}_0,R)=\begin{cases} c(R^2-\|\mathbf{x}-\mathbf{x}_0\|^2)^2, & \|\mathbf{x}-\mathbf{x}_0\|^2<R^2,\\ 0, & \text{otherwise,}\end{cases} \tag{7}$$

where $\mathbf{x}_0$ is the centre of the NEF, R its radius and c is a normalisation constant. The NEF corresponding to the centre $\mathbf{x}_0=(16,16)$ with radius $R=8$ is shown in Fig. 6. Each NEF is normalised such that the integral of the square of the function Φ over the entire field is equal to unity

$$\int \Phi^2(\mathbf{x})\,\mathrm{d}^2\mathbf{x}=1. \tag{8}$$

Suppose that the temperature field $\mathbf{G}$ at a particular time is approximated by a linear combination of K NEFs

$$\hat{\mathbf{G}}^{(K)}=\sum_{k=1}^{K} a_k\Phi_k. \tag{9}$$

As K increases the approximation improves.

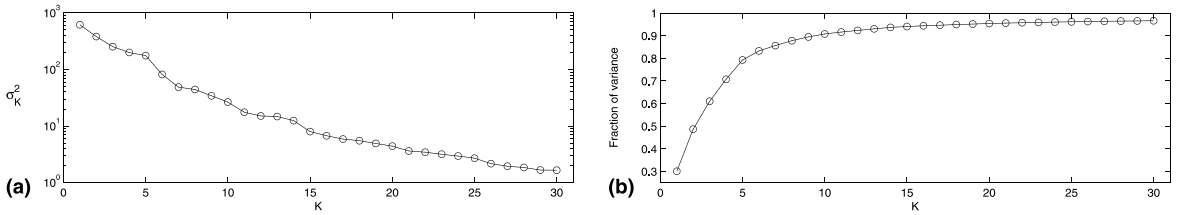

Fig. 5. EOF reconstruction: (a) singular value spectrum; (b) fraction of variance explained, both as a function of the number of EOFs used for reconstruction.

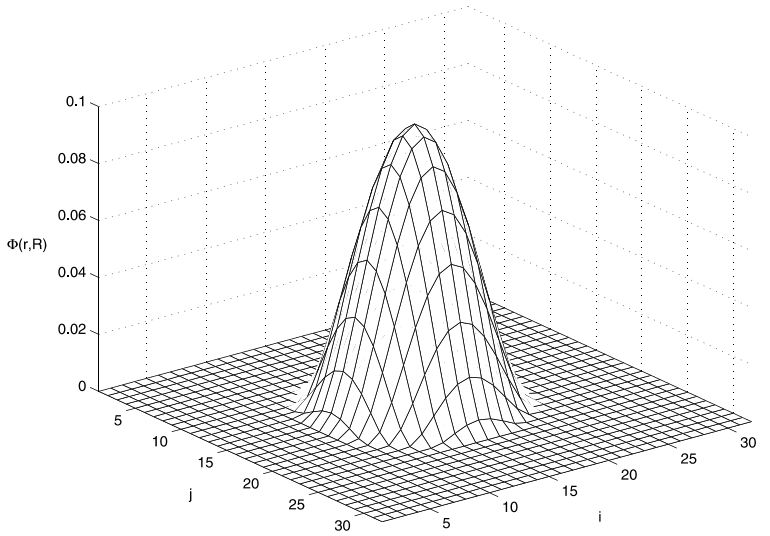

Fig. 6. NEF basis function $\Phi(\mathbf{x};\mathbf{x}_0,R)$ with $\mathbf{x}_0=(16,16)$ and $R=8$.

Given a temperature field $\mathbf{G}$ and a model structure such as (9), the coefficients a_k can be determined using a maximum likelihood approach [39]. If the measurement errors are independent and normally distributed, then the maximum likelihood principal reduces to least squares [39], i.e., minimises

$$C_{\mathrm{LS}}=\frac{1}{M}\mathbf{E}^{(K)^{\mathrm{T}}}\mathbf{E}^{(K)}, \tag{10}$$

where $\mathbf{E}^{(K)}=\mathbf{G}-\hat{\mathbf{G}}^{(K)}$ is the model reconstruction error which results from using K basis functions. The fact that $\hat{\mathbf{G}}^{(K)}$ is linear in the coefficients implies that a unique solution may be obtained using singular value decomposition [36].

For the EOFs, one often selects a target fraction of the variance and keeps the required number of EOFs. For NEFs, a number of criteria exist for quantifying the optimal model size K. The quantity C_{LS} defined in (10) can be used as a criterion to decide when to stop increasing K. The complexity of a model $\hat{\mathbf{G}}$ may be taken into account by multiplying (10) by a penalty term [40],

$$C(K)=\frac{1}{M}\mathbf{E}^{(K)^{\mathrm{T}}}\mathbf{E}^{(K)}\exp(\alpha K), \tag{11}$$

so that models with fewer parameters (smaller K) are favoured by the selection criteria. In particular, Rissanen [41,42] derives an expression based on a minimal description length argument [43], $\alpha=(\ln M)/2M$.

The non-orthogonality of a NEF basis implies that the construction of increasing orders of approximation is no longer sequential; the approximation of order $K+1$ is affected by terms of order less than K. An iterative procedure is therefore required to construct the model $\hat{\mathbf{G}}$.

Let $\mathscr{V}$ represent a pool of normalised basis functions Φ_k, including a constant NEF, $\Phi(\mathbf{x})=\text{const}$. Judd and Mees [43,44] construct a model $\hat{\mathbf{G}}^{(K)}$ by iteratively selecting a set $\mathscr{B}$ of K basis function indices from $\mathscr{V}$. A sensitivity analysis [43] may be used to quantify the effect of adding one new basis function to $\mathscr{B}$. Let $\boldsymbol{\mu}=-\mathscr{V}^{\mathrm{T}}\mathbf{E}^{(K)}$ be the projection of the error field onto the entire pool of basis functions. The largest element of $\boldsymbol{\mu}$ in absolute value is the index which should be added to the basis to give the largest marginal improvement to the approximation. Similarly, sensitivity analysis suggests that, when removing a basis function from $\mathscr{B}$, removing the basis function corresponding to the smallest coefficient a_k will do the least damage to the approximation. These two observations provide a method of selecting a good representation of the data with K basis functions by adding, then deleting, basis functions until the basis set no longer changes. Details of the algorithm are given in Appendix A.

Fig. 7 demonstrates the procedure of obtaining a NEF reconstruction of the single temperature field shown in the top left panel (the same as the first field in Fig. 1). The first NEF used is constant over the field and is chosen to remove the baseline of the field. Subsequent panels show the reconstructions obtained using additional basis functions while attempting to minimise the cost function given by (10). Note that both negatively and positively weighted basis functions are used. Since the analysed field represents just a small area of the stainless steel plate where boiling occurred, it is possible that nucleation sites outside the sample area contributed to temperature changes inside. For this reason, NEF centres were given the freedom to position themselves

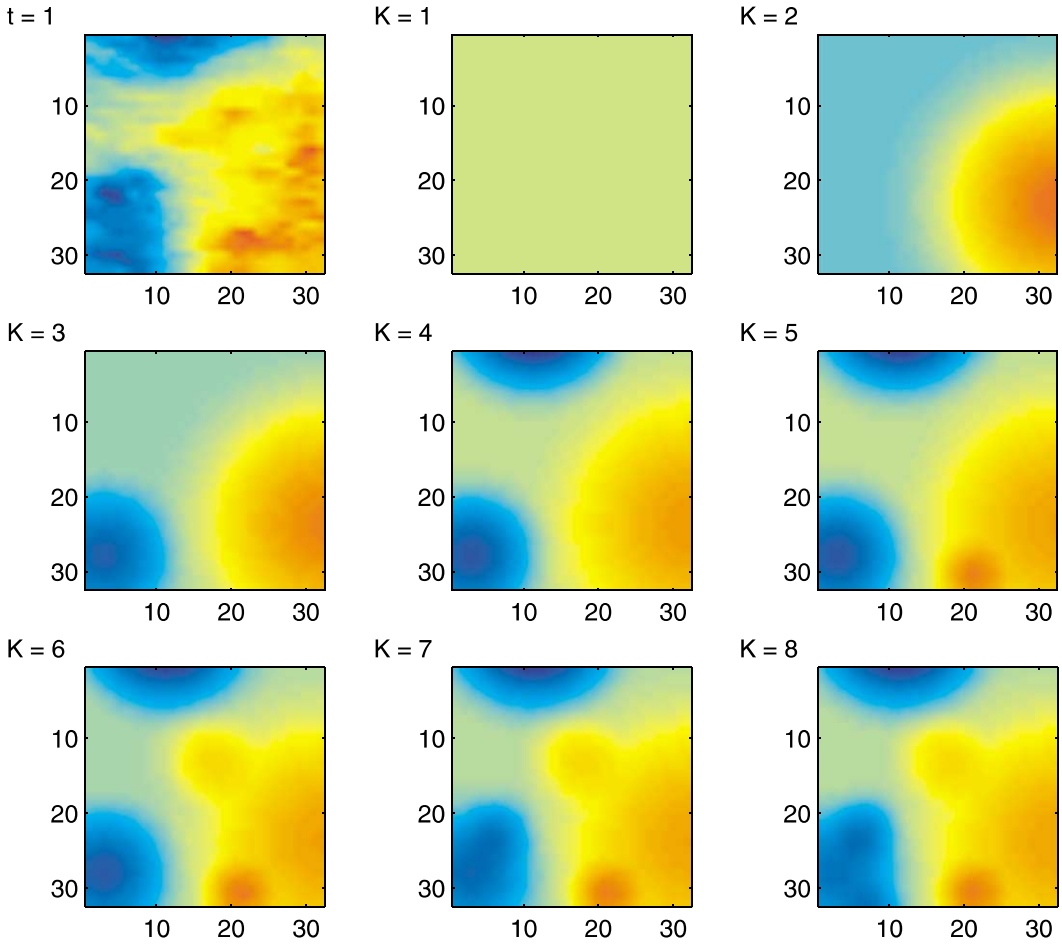

Fig. 7. Demonstration of the procedure for constructing the NEF representation (9) of the first temperature field (shown in top left panel). Subsequent panels show the approximations achieved using $K = 1, 2, \ldots, 8$ NEFs. Colour map as in Fig. 1.

both on the sample (32×32 pixels) and on a boundary perimeter which was 10 pixels in width.

The number of NEFs used depends on the penalty term used in the cost function (11). In the limit as $\alpha \to 0$, the number of NEFs used would tend to M as no cost would be given to the complexity of the reconstruction needed to replicate the true field. In the analysis reported here, a penalty weighting value of $\alpha = 40(\ln M)/M$ was chosen in (11).

In the last panel of Fig. 7, the reconstruction with eight NEFs, some negative and some positive, bears some resemblance to the original temperature field. The penalty term in the cost function (11) has the effect of controlling the number of basis functions chosen. Otherwise more and more basis functions would be added as the reconstruction converges to the true field. The accuracy required depends on the purpose of the analysis: a small number of NEFs may be sufficient to identify nucleation sites, more may be needed to specify the temperature at each site at the instant of nucleation. The later members of the set may carry information unrelated to the nucleation sites, e.g., other sources of convective heat transfer or noise in the experimental data. As already discussed for EOFs in Section 4, the truncation of the set of NEFs may also be used as a way of filtering noise.

6. Results of NEF analysis

The reconstruction illustrated in Fig. 7 must be applied separately to every temperature field. The centres and radii of the NEFs used to reconstruct the nine consecutive fields in Fig. 1 are shown in Fig. 8. NEFs with negative weights are shown as blue circles, whereas NEFs with positive weights have red circles. In all cases the technique has placed negative NEFs at positions corresponding to the centres of large drops in tempera-

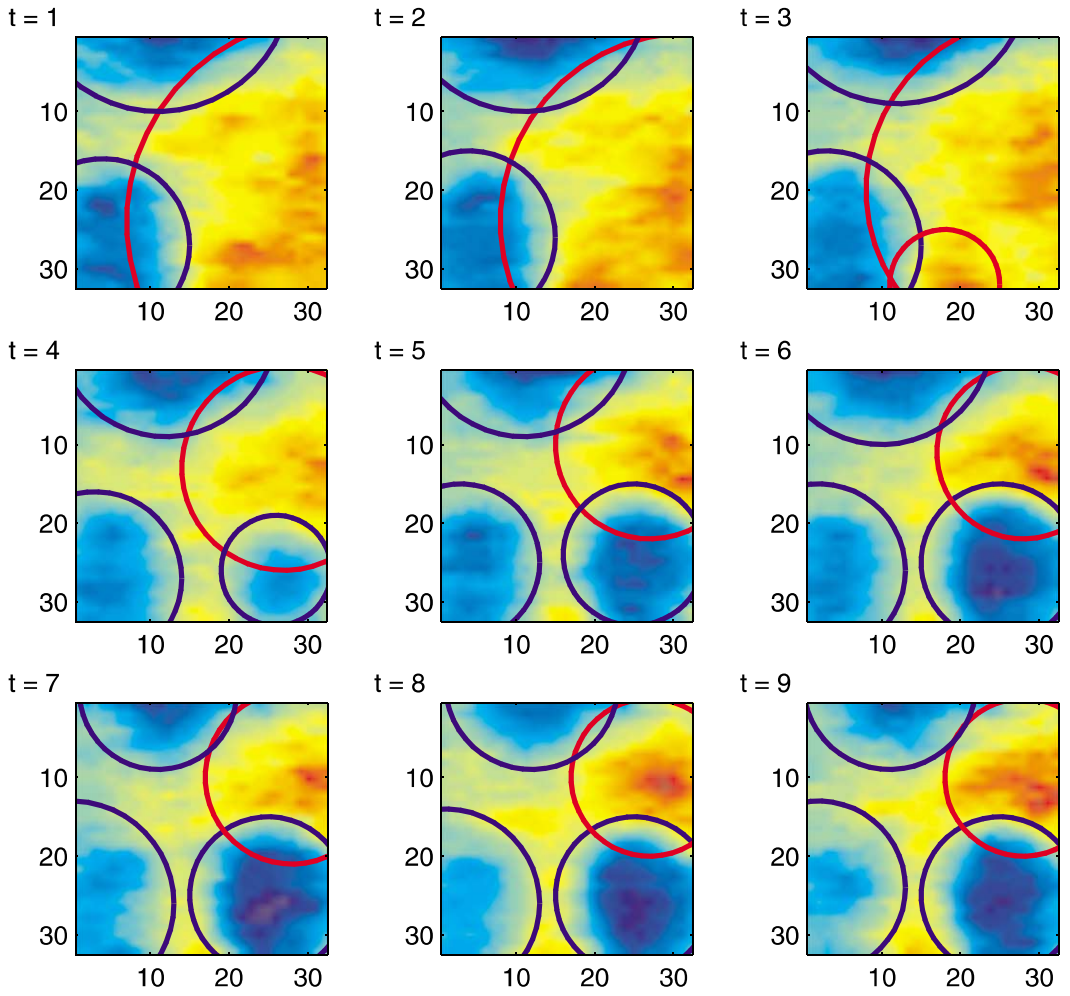

Fig. 8. An illustration of the positions and radii chosen for the NEFs during the first nine time steps. NEFs with negative weights are shown in blue, while those with positive weights are shown in red. Colour map as in Fig. 1.

ture, which are likely to be associated with nucleation sites. Between three and four non-constant NEFs are required in the reconstruction of each field in Fig. 8.

Fig. 9(a) shows a histogram of the number of NEFs used for reconstruction when the analysis is extended to all N fields, with the numbers of negatively and positively weighted NEFs shown separately in Figs. 9(b) and (c), respectively. Note that decreasing α in (11) would have the effect of shifting these histograms to larger values.

The distribution of NEF radii sizes is shown in Fig. 10. This indicates that the most common radius is around 12 pixels. Note that since bubbles survive for several time steps, often with varying radii, this histogram cannot give a clear indication of the typical *bubble* size distribution. This latter distribution could be obtained by following the evolution of single bubbles in time and such a "bubble census" will be discussed in a future paper.

Fig. 11 shows a histogram of the centre positions of negatively weighted NEFs. The distribution shows a sharp peak around position $(6, 27)$, a broader peak around $(27, 30)$ and a significant but broad distribution in the top perimeter region. In addition, there are many positions which occur only a few times during the sequence of 8000 frames. Caution is required in using these distributions alone to identify the positions of active sites. The argument for the form of the function used for the NEF analysis is that negative centres are likely to be associated with nucleation sites but some negative NEFs may also be required to represent additional mechanisms of cooling, such as convection that is not related to a single bubble. When cooling is caused by a nucleating bubble, it persists for many frames, leading to a sequence of NEFs with the same (or nearly the same) centres, as in Fig. 8. Thus there is some ambiguity about the interpretation of a negative centre with

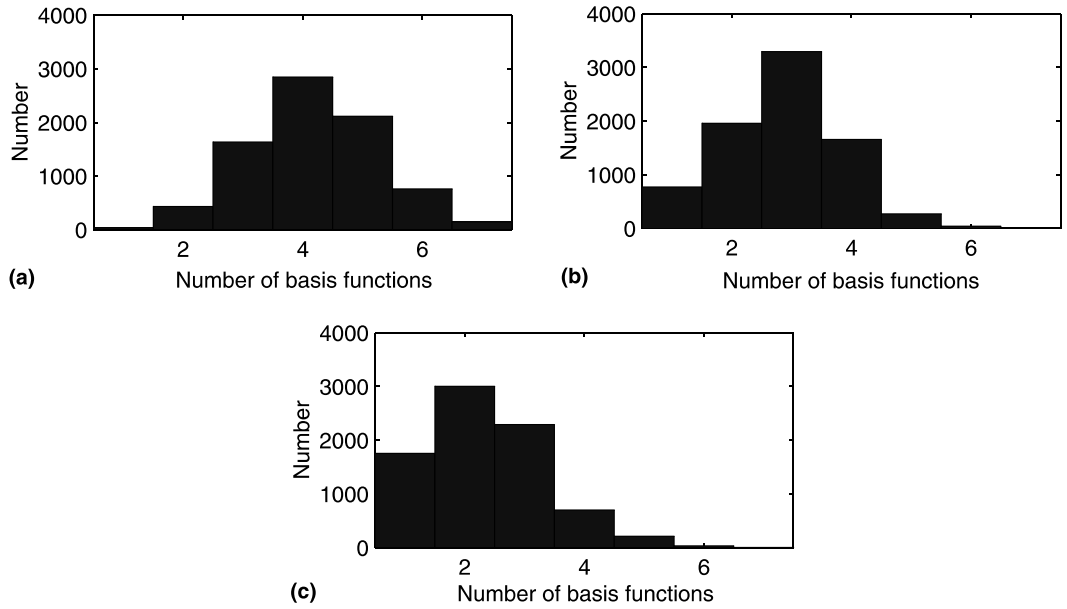

Fig. 9. Histogram of the number of non-constant NEFs needed for the reconstruction at each of the time steps for (a) all values of a; (b) $a < 0$; (c) $a > 0$.

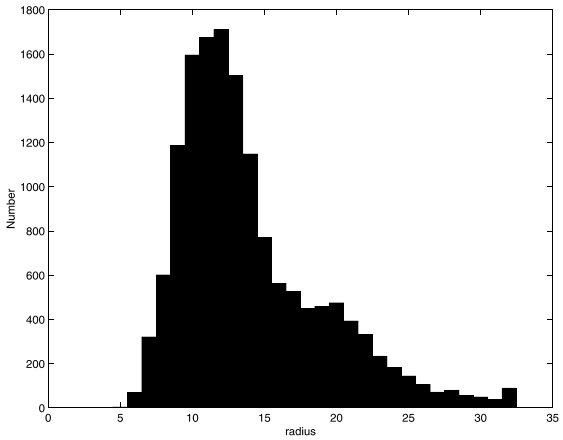

Fig. 10. Histogram of the radii sizes use at each time step calculated over all time steps for $a < 0$.

only a few occurrences: it may not be a nucleation site at all, or it may be a site that produces only one or two short-lived bubbles during the period of the data analysis. Other physical processes may influence the distributions:

- One site may actually be a group of cavities with almost the same activation superheats, closely spaced relative to the bubble radius (i.e., within one or two pixels of each other in this study), which share bubble production. The sites identified in [1] exhibited some scatter and were consolidated on this length scale and this is one possible explanation for the small variations in activation superheat for different bubbles at the same site in [11,12]. The definition of a single site for modelling purposes may then depend on the relative size of the scales of surface micro-roughness and bubble radius, which depends on system pressure (see [3,4]).
- Other sites may be closely spaced but have different activation superheats, so that they interact with each other and cause intermittency, as described in [1,16]. This may be the case for the site at $(25, 25)$ in Fig. 8 and what appears to be a much more active site at $(27, 30)$ in Fig. 11.

One of the objectives of the analysis is to detect and eventually quantify the significance of these interactions, which requires the additional information about the weights a and radii R of the NEFs and their resolution in time, not included in Fig. 11. A first attempt at this sort of analysis over a short time interval of 200 time steps is presented graphically in Fig. 12, where the radii of the circles represent the weighting function (temperature drop) and the radius R in panels (a) and (b) respectively. From physical arguments, bubble nucleation is expected to cause a temperature drop that increases rapidly in magnitude and then declines. The position of the nucleation site can be found most accurately from the NEF at the start of the temperature drop. In Fig. 12(a), it is possible to identify bubbles growing at $(27, 6, t = 110)$, $(27, 6, t = 150)$, $(27, 30, t = 0)$, $(27, 30, t = 140)$ and at the less active site $(15, 15, t = 50)$; in addition there is a lot of activity at sites in the top perimeter region, as anticipated from Fig. 11. There is a tendency for the centres of

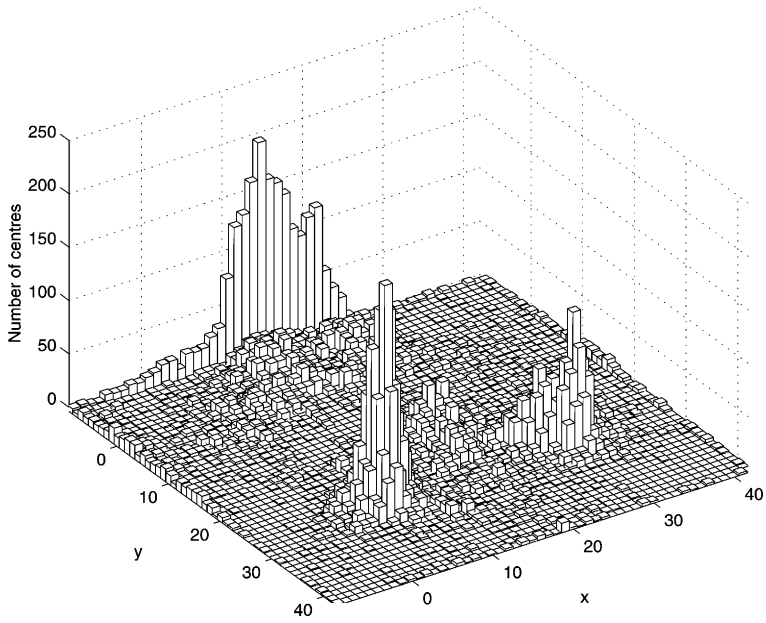

Fig. 11. Histogram showing the spatial positions of NEF centres. This includes only those centres for which the weights a_k are negative.

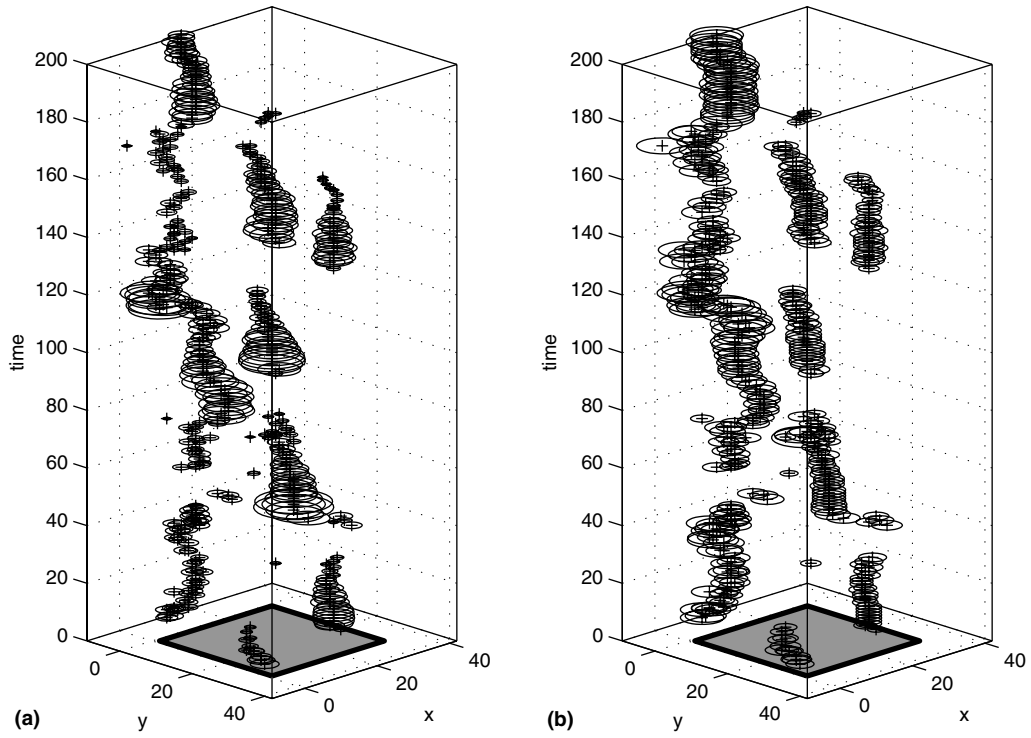

Fig. 12. Evolution of centre positions of negatively weighted basis functions over first 200 time steps. The radii of the circles shown are proportional to: (a) the coefficients a; (b) the radii R of the NEF reconstructions. The shaded square reflects the area from which the temperature fields were recorded.

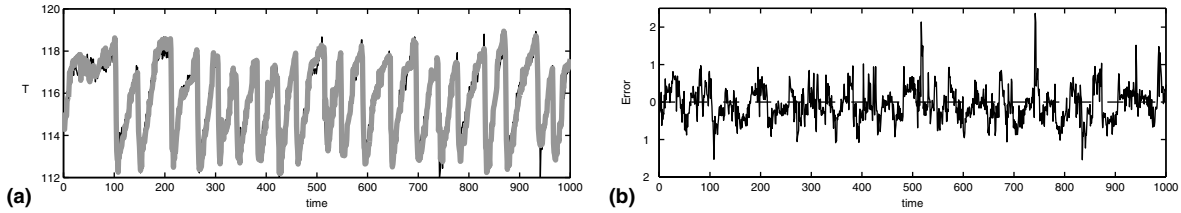

Fig. 13. Comparison of observed temperature and NEF reconstructed temperature at pixel $(6, 27)$: (a) observed temperature (black line), NEF reconstruction (grey line); (b) NEF reconstuction error. Temperatures and errors are in °C and time is expressed as the number of time steps.

the NEFs in each bubble sequence to drift sideways with increasing time. This contributes to the spread of centres in Fig. 11 and suggests that there is an additional physical process at work that has a general influence on the heat transfer around nucleation sites after bubbles have departed, perhaps the flow circulation in the boiling cell. Circulation was observed in [1] through the general pattern of motion of the bubbles but no effect was detected in the studies of temperature fields after the departure of individual bubbles. The reconstruction by EOFs in Fig. 4 is not capable of giving a clue to the possible existence of this effect.

The physical processes of nucleate boiling are expected to be particularly sensitive to the superheats at the nucleation sites, which must therefore be reconstructed accurately. A section of the temperature–time series for the site at $(27, 6)$ is shown in Fig. 13. Even for the small number of NEFs used in this study (between one and six per field because of the setting of the cost function), the differences between the original and reconstructed data have a standard deviation $\simeq 0.5$°C, which is about the same as the accuracy of the original measurements.

7. Discussion and future work

Understanding the interactions between nucleation sites in boiling requires the digestion of large quantities of spatio-temporal data. In other branches of the physical sciences, one of the tools used to approach this task is PCA. While EOFs are by construction optimal for capturing variance within the data, capturing the variance need not lead to a natural physical interpretation, as discussed in Section 4. NEFs provide a more natural description of boiling data in terms of cooling and superheating regions. As shown in the previous section, this description allows for the analysis of spatial and temporal correlations between nucleation events, for their statistical characterisation and for the analysis of the dynamics of single nucleation events. Such an analysis of local features is not straightforward in the PCA framework.

Another weakness of PCA when applied to non-linear dynamics is that individual members of the EOF basis are rarely independent. The constraint of orthogonality ensures that they are not linearly correlated, but it fails to address non-linear correlations. PCA fails to distinguish sporadic, intermittent nucleation events and background noise with the same variance; these are clearly distinguished in the NEF analysis. NEF anlaysis is more robust to non-stationarity than PCA, as NEFs deal with each time frame independently; given a change in heat flux, the NEFs could adapt to new nucleation sites at the cost of having to use additional NEFs.

When data compression is of interest, NEFs provide an extremely compact representation. While EOFs are fixed at all times, NEFs are allowed to vary at each time step, so they can effectively compete with EOFs also in terms of variance compression. For example the NEF analysis of the dataset presented in this paper achieves a time-averaged reconstruction error (see Eq. (10)) of $\bar{C}_{\mathrm{LS}} = \frac{1}{N}\sum_i C_{\mathrm{LS}}(t_i) = 0.29°\mathrm{C}^2$, equivalent to 15% of the variance, using an average of four NEFs per time step (see Fig. 9(a)). As shown in Fig. 5, at least seven EOFs are necessary to obtain the same compression. Even though the NEF representation requires the specification of the indices of the NEFs used at each time step, this overhead is compensated in this application by the smaller average number of NEFs per frame, compared to the number of EOFs required to obtain the same compression. More important than compressing variance, however, the NEFs transmit more relevant information: the location and strength of nucleation sites in each frame.

To summarise, this work has demonstrated the successful application of a new method of analysis by NEFs to data for the spatio-temporal wall temperature fields measured by liquid crystal thermography during nucleate boiling on a horizontal plate. It has been shown that the method has advantages over more conventional methods using EOFs in its applicability to non-stationary processes for capturing single nucleation events and the directness of its physical interpretation.

So far the method has been applied to data from a small array of pixels and analysis of the temporal evolution of the fields has not been fully implemented.

The next stage is to apply the temporal analysis to data from larger arrays, in order to investigate the interactions between a large group of nucleation sites over a long time period.

While there are many statistical approaches to modelling data from physical systems, few of these attempt to hardwire known physical constraints into the modelling technique. In the case of nucleate pool boiling on a horizontal plate, it has been shown that the assumption of radially symmetric NEFs is a good approximation to the temperature field obtained during bubble formation at a nucleation site. The approach presented in this paper focuses on patches of the field displaying large temperature decreases in order to identify the underlying nucleation sites. The method should also work when the physics of boiling indicate that asymmetrical NEFs such as ellipses might be more appropriate, e.g., when the bubbles have a component of velocity tangential to the surface in boiling on vertical [11,12] or sloping [13] plates, or in the presence of an external flow field. NEFs are especially advantageous when their shape is matched to particular localised physical processes, but they are also able to represent fields which include processes with other characteristic shapes.

In addition to spatial correlations, the NEF analysis can utilise the obvious correlations that exist over time due to the bubbles lasting longer than a single time step. The present algorithm will be extended to incorporate these temporal correlations in future work. It is expected that such modifications will improve the accuracy of the nucleation site identification algorithm presented here.

In general, whenever physical insight suggests that either spatial correlations of temporal evolution will not be linear, one may expect a NEF approach to outperform EOF approaches.

Acknowledgements

This work was supported by Engineering and Physical Science Research Council grants GR/K99305, GR/M89034 and equipment from the EPSRC Loan Pool, and ONR grant N00014-99-1-0056. PEM received a Marie Curie Research Fellowhip from the European Community under grant ERBFMBICT950203. JHE received scholarships from the Harold Hyam Wingate Foundation and Lincoln College, Oxford. LAS was supported by Pembroke College, Oxford.

Appendix A

The following is an algorithm for implementing the basis selection technique introduced by Judd and Mees [43,44] for the selection of NEFs. All the symbols used are also defined in Section 5. Given a field of measurements $\mathbf{G}(t)$, the algorithm aims at finding a reconstruction (9), choosing a set of K basis functions $\mathscr{B}$ from a large pool $\mathscr{V}$ of L possible normalised basis functions.

The number of basis functions in the basis, K, is chosen such that the cost function $C(K)$ given in (11) is minimised. In the following, each NEF in $\mathscr{V}$ is identified by an index $i = 1, \ldots, L$. $\mathbf{E}^{(K)} = \mathbf{G} - \hat{\mathbf{G}}^{(K)}$ is the model reconstruction error which results from using K basis functions in $\mathscr{B}$.

(i) Let $\mathscr{B}$ initially be an empty set and $k = 1$ the number of NEFs to be included in the basis in this iteration. Define $\mathbf{E}^{(0)} = \mathbf{G}$.

(ii) Let $\boldsymbol{\mu} = -\mathscr{V}^{\mathrm{T}}\mathbf{E}^{(k-1)}$ be the projection of the reconstruction errors onto the pool of basis functions. Let i_{in} be the index (in $\mathscr{V}$) of the component of $\boldsymbol{\mu}$ with maximum absolute value. This is the NEF which will be included in the basis, $\mathscr{B} = \mathscr{B} \cup \{i_{\mathrm{in}}\}$. Note that typically the constant NEF, $\Phi(\mathbf{x}) = \text{const.}$, will be selected initially (when $K = 1$).

(iii) Calculate the coefficients $a_{\mathscr{B}}$ associated with all the NEFs in the basis $\mathscr{B}$ so far, see (9). Let i_{out} be the NEF having the coefficient with smallest absolute value. This NEF is a candidate for removal from the basis.

(iv) If $i_{\mathrm{in}} \neq i_{\mathrm{out}}$, then remove i_{out} from the basis, $\mathscr{B} = \mathscr{B} \setminus \{i_{\mathrm{out}}\}$, and go to step (ii).

(v) Store the current $\mathscr{B}^{(k)} = \mathscr{B}$ and calculate the cost function $C(k)$, see (11).

(vi) If $C(k) < C(k-1)$, then increase $k = k + 1$ and go to step (ii).

(vii) The selected basis is that having the minimum cost function, $\mathscr{B}^{(K)}$, $K = k - 1$.

References

[1] D.B.R. Kenning, Y. Yan, Pool boiling heat transfer on a thin plate: features revealed by liquid crystal thermography, Int. J. Heat Mass Transfer 39 (15) (1996) 3117–3137.

[2] D. Gorenflo, Behältersieden, fourth ed., Kap. Ha, VDI, Wärmeatlas, Düsseldorf, 1984.

[3] D. Gorenflo, A. Luke, E. Danger, Interactions between heat transfer and bubble formation in nucleate boiling, in: Proceedings of the 11th International Heat Transfer Conference, vol. 1, Kyongju, 1998, pp. 149–174.

[4] A. Luke, E. Baumhögger, P. Scheunemann, 3-dimensional description of the microstructure of heated surfaces in nucleate pool boiling, in: Proceedings United Engineering Foundation Conference Boiling 2000, vol. 1, Alaska, 2000, pp. 136–151.

[5] D.B.R. Kenning, Experimental methods; looking closely at bubble nucleation, in: Proceedings United Engineering Foundation Conference Boiling 2000, vol. 1, Alaska, 2000.

[6] M.M. Mikic, W.M. Rohsenow, A new correlation of pool boiling data including the effect of heating surface characteristics, Trans. ASME J. Heat Transfer 91 (1969) 245–250.
[7] H. Beer, P. Burow, R. Best, Bubble growth, bubble dynamics and heat transfer in nucleate boiling, in: E. Hahne, U. Grigull (Eds.), Heat Transfer in Boiling, Hemisphere, Washington, 1977 (Chapter 2).
[8] Z. Guo, M.S. El-Genk, Liquid microlayer evaporation during nucleate boiling on the surface of a flat composite wall, Int. J. Heat Mass Transfer 37 (1994) 1641–1655.
[9] R. Mei, W. Chen, J.F. Klausner, Vapor bubble growth in heterogeneous boiling – I. Formulation, Int. J. Heat Mass Transfer 38 (1995) 909–919; R. Mei, W. Chen, J.F. Klausner, Vapor bubble growth in heterogeneous boiling – II. Growth rate and thermal fields, Int. J. Heat Mass Transfer 38 (1995) 921–934.
[10] A.A. Watwe, D.K. Hollingsworth, Liquid crystal images of surface temperature during incipient pool boiling, Exp. Therm. Fluid Sci. 9 (1) (1994) 22–33.
[11] M. Wienecke, Y. Yan, D. Kenning, Bubble nucleation and growth during saturated pool boiling on a thin vertical plate, in: L.M.D. Mewes (Ed.), Applied Optical Measurements, Springer, Berlin, 1999.
[12] D.B.R. Kenning, T. Kono, M. Wienecke, Investigation of boiling heat transfer by liquid crystal thermography, in: Proceedings of the Joint ASME-ZSITS International Thermal Science Seminar, vol. 1, Bled, 2000, pp. 35–46.
[13] Y. Yan, D.B.R. Kenning, K. Cornwell, Sliding and sticking bubbles under inclined plane and curved surfaces, Int. J. Refrig. 20 (1997) 583–591.
[14] I. Golobic, E. Pavlovic, S. Strgar, D.B.R. Kenning, Y. Yan, Wall temperature variations during bubble growth on a thin plate: computation and experiment, in: Proceedings of the Eurotherm Seminar No. 48, Pool Boiling 2, Paderborn, Germany, 1996, pp. 25–32.
[15] R.L. Judd, A. Chopra, Interaction of the nucleation processes occurring at adjacent nucleation sites, Trans. ASME J. Heat Transfer 115 (1993) 962–995.
[16] P.E. McSharry, L.A. Smith, T. Kono, D.B.R. Kenning, Nonlinear analysis of site interactions in pool nucleate boiling, in: Proceedings of the 3rd European Thermal Sciences Conference, vol. 2, Heidelberg, Germany, 2000, pp. 725–730.
[17] K.O. Pasamehmetoglu, R.A. Nelson, Cavity-to-cavity interaction in nucleate boiling: the effect of heat conduction within the heater, in: AIChE Symposium Series (27th National HT Conference, Minneapolis, USA), vol. 87, 1991, pp. 342–351.
[18] C. Unal, K.O. Pasamehmetoglu, A numerical investigation of the effect of heating methods on saturated nucleate boiling, Int. Comm. Heat Mass Transfer 21 (1994) 167–177.
[19] I. Golobic, E. Pavlovic, S. Strgar, Computer model for nucleation site interactions on a thin plate, in: Proceedings of the Eurotherm Seminar No. 48, Pool Boiling 2, Paderborn, Germany, 1996, pp. 33–42.
[20] C. Sadasivan, P. Unal, R.A. Nelson, Nonlinear aspects of high heat flux nucleate boiling heat transfer, Trans. ASME J. Heat Transfer 117 (1995) 981–988.
[21] Y. He, Numerical simulation of high heat flux pool boiling heat transfer, Ph.D. Thesis, Department of Mechanical Engineering, University of Tokyo, 1999.
[22] A. Luke, T. Runowski, Heat transfer and size distribution of active nucleation sites in boiling hydrocarbons, in: Proceedings of the Engineering Foundation Conference on Convective Flow and Pool Boiling, Irsee, Germany, 1997, pp. 89–96.
[23] M. Mann, K. Stephan, Influence of convection on nucleate boiling heat transfer around horizontal tubes, in: Proceedings of the United Engineering Foundation Conference Boiling 2000, vol. 1, Alaska, 2000, pp. 171–185.
[24] K. Tajima, M. Shoji, Mathematical simulation model of boiling – boiling modes and chaotic features, in: Proceedings of the Engineering Foundation Conference on Convective Flow and Pool Boiling, Irsee, Germany, 1997, pp. 217–222.
[25] T. Yanagita, Phenomenology for boiling: a coupled map lattice model, Chaos 2 (1993) 343–350.
[26] L.A. Smith, The maintenance of uncertainty, in: G. Cini (Ed.), Nonlinearity in Geophysics and Astrophysics, Vol. CXXXIII, International School of Physics ''Enrico Fermi'', Società Italiana di Fisica, Bologna, Italy, 1997, pp. 177–246.
[27] L.A. Smith, Disentangling uncertainty and error: on the predictability of nonlinear systems, in: A.I. Mees (Ed.), Nonlinear Dynamics and Statistics: Proceedings of an Isaac Newton Institute, Birkhäuser, Boston, 2000, pp. 31–64.
[28] R.A. Nelson, D.B.R. Kenning, M. Shoji, Nonlinear dynamics in boiling phenomena, J. Heat Transfer Soc. Jpn 35 (1996) 22–34.
[29] M. Shoji, T. Kono, N. Negishi, S. Tayoshima, A. Maeda, Chaos in boiling on a small-size heater, in: Proceedings of the ASME/JSME Thermal Engineering Conference 2, Kyongju, 1995, pp. 233–238, see also Ref. [31].
[30] D.J. Lee, Regular–irregular bubble departure patterns of film boiling on a horizontal heating wire, Int. Comm. Heat Mass Transfer 24 (1997) 1039–1048.
[31] M. Shoji, H. Hatae, Y. Haramura, Nonlinear characteristics of boiling, in: Proceedings of the 33rd Japan National Heat Transfer Symposium 1, 1996, pp. F114, 253–254 (in Japanese).
[32] J.H. Ellepola, Nucleate boiling: nonlinear spatio-temporal variations in wall temperature, Ph.D. Thesis, Department of Engineering Science, University of Oxford, 1997.
[33] J.H. Ellepola, D.B.R. Kenning, Nucleation site interactions in pool boiling, Proceedings of the 2nd European Thermal-Sciences and 14th UIT National Heat Transfer Conference 3 (1996) 1669–1675.
[34] J.H. Ellepola, P. McSharry, D.B.R. Kenning, Is nucleate boiling choatic? (and who cares?), in: Proceedings of the Eurotherm Seminar No. 48, Pool Boiling 2, Paderborn, Germany, 1996, pp. 17–24.
[35] D.S. Broomhead, G.P. King, Extracting qualitative dynamics from experimental data, Physica D 20 (1986) 217–236.
[36] W.H. Press, B.P. Flannery, S.A. Teukolsky, W.T. Vetterling, Numerical Recipes in C, second ed., Cambridge University Press, Cambridge, 1992.

[37] C. Bishop, Neural Networks for Pattern Recognition, Oxford University Press, New York, 1995.
[38] G. Strang, Linear Algebra and its Applications, Harcourt College Publishers, San Diego, 1988.
[39] P.E. McSharry, L.A. Smith, Better nonlinear models from noisy data: attractors with maximum likelihood, Phys. Rev. Lett. 83 (21) (1999) 4285–4288.
[40] H. Kantz, T. Schreiber, Nonlinear Time Series Analysis, Cambridge University Press, Cambridge, 1997.
[41] J. Rissanen, Consistent order estimates of autoregressive processes by shortest description of data, in: Analysis and Optimisation of Stochastic Systems, Academic, New York, 1980.
[42] J. Rissanen, Stochastic Complexity in Statistical Inquiry, vol. 15, World Scientific, Singapore, 1989.
[43] K. Judd, A. Mees, On selecting models for nonlinear time series, Physica D 82 (1995) 426–444.
[44] K. Judd, A.I. Mees, Modeling chaos from experimental data, in: K. Judd, A.I. Mees, K.L. Teo, T. Vincent (Eds.), Control and Chaos, Birkhäuser, Boston, 1997, pp. 25–38.